Recent Res. Devel. Physical Chem., 3 (1999): 261-275

# Molecular dynamics simulations of crystallization: Molecular liquids

**Igor M.Svishchev and Peter G. Kusalik**
Department of Chemistry, Trent University, Peterborough, Ontario, K9J 7B8, Canada./Department of Chemistry , Dalhousie University, Halifax, Nova Scotia, B3H 4J3, Canada

## ABSTRACT

Crystallization of molecular liquids has many practical consequences, yet our understanding of this process at the microscopic level is rather limited. Recent computational advances made in the study of crystallization of liquids are reviewed with emphasis placed on molecular systems. Molecular dynamics simulation method is described. Novel results concerning the microscopic dynamics of crystallization of a nonpolar molecular liquid, carbon dioxide, are presented. Crystallization of a polar liquid, water, is discussed, mainly in the context of electric field induced ice nucleation.

## 1. INTRODUCTION

The crystallization of a liquid is a common phenomenon which occurs in many natural and technological processes. Controlling this process is important in many areas of materials science. Yet our understanding of this process at the microscopic level is rather fragmented.

Thermodynamics views the transformation of a liquid into a crystal as a first-order phase transition. In the absence of a foreign surface or particle to promote heterogeneous nucleation, this phase transition begins with the spontaneous nucleation of atoms (ions) or molecules into small aggregates which, if they reach a critical size, form the seeds for the new phase. Unfortunately, experimental techniques can not provide much information about individual nucleation events which occur on a sub-microsecond time-scale with critical nuclei having liner dimensions of a few nanometers. That leaves us with a simulation as a primary source of microscopic information.

Over the past two decades computer simulations have provided us with a picture of the crystallization of simple monoatomic liquids by directly probing the microscopic dynamics of this phase transition (1-3). However, rather limited success has been reported for molecular systems. The crystallization of a molecular liquid, in contrast to a melting of a molecular solid, has not been readily observable in computer simulations.

A simple explanation can be summoned. Crystallization is an activated process, a transition between two stable states (i.e. liquid and regular solid) separated by a region of metastability, and it

can be viewed as a crossing of the free energy barrier (or a series of barriers) in the phase space (4). When the free energy barriers are much higher than kT, and when the liquid state trajectory encounters a "maze" of metastable glassy "traps" which encompass a global minimum domain (representing the crystalline state), the crossing is an infrequent event. The glassy states which emerge upon reducing the temperature usually prevent a spontaneous nucleation of a molecular heterophase within the time-scale of a typical simulation. Although the crystallization of a simple Lennard-Jones fluid was first studied more than 20 years ago (5), only recently has the crystallization of molecular fluids been observed in a computer simulation (6, 7).

This paper reviews some recent advances made in the study of the crystallization of molecular liquids using computer simulations. Our focus will be on the freezing of bulk liquids, the crystallization of molecular clusters is described elsewhere (8). Theoretical aspects of liquid-solid transition (the nucleation theories) have been extensively covered in earlier reviews (9, 10). The reminder of this paper is organized as follows. In Section 2 we present a very brief introduction into molecular dynamics (MD) simulation method. The crystallization of nonpolar molecular liquids is discussed in Section 3. Section 4 describes a method for an enhanced configurational sampling in MD simulations of the crystallization. Then, in Section 5 we focus upon the phenomenon of the electric field induced ice nucleation (the electrofreezing of water). Finally, our concluding remarks can be found in Section 6.

## 2. MOLECULAR DYNAMICS SIMULATIONS

Molecular Dynamics simulation deals with the motions of a system of individual particles with respect to the forces that are present in the system (11, 12). In this method the positions of particles are obtained by numerically solving differential equations of motion. The positions are connected in time and, hence, reveal the microscopic dynamics of a system.

MD simulation consists of three principal steps: (a) construction of a molecular model (intermolecular potential), (b) calculation of molecular trajectories and (c) analysis of dynamical trajectories to obtain physical-chemical properties.

As a first step in performing a simulation one must choose a functional form for the intermolecular potential. Very often (but not always) the potential is assumed to be pairwise additive, i.e. the interactions in the system can be written as a sum of isolated two-body contributions:

$$U(r^N) = \sum_{i<j}\sum u_{ij}, \qquad (1)$$

where $U(r^N)$ is the total intermolecular potential function and $u_{ij}$ is the pair potential.

We may remark that although rather complex potential functions exist (accounting for molecular flexibility and quantum effects, for example), simplicity has remained a very desirable trait of any interaction model employed in a computer simulation. Clearly, the fact that very long simulation runs are usually necessary if collective quantities such as the relaxation (nucleation) times or the dielectric constant are required remains an important consideration.

For instance, among water potentials the rigid point charge models such as SPC/E (simple point charge), TIP4P (transferable intermolecular potential) and PPC (polarizable point charge) appear to yield various physical properties close to that of the true

system (13 -15).

For non-polarizable water models, such as SPC/E or TIP4P, the effective pair potentials can be written as

$$u_{ij} = u_Q + u_{LJ} , \qquad (2)$$

where

$$u_Q = \sum_k^{on\,i} \sum_l^{on\,j} \frac{Q_k Q_l}{r_{kl}} \qquad (3)$$

is the Coulomb term in which the summation is carrying over the site charges k and l on the molecules i and j, respectively, and

$$u_{LJ} = 4\varepsilon_{LJ}\left[\left(\frac{\sigma}{r_{ij}}\right)^{12} - \left(\frac{\sigma}{r_{ij}}\right)^{6}\right] \qquad (4)$$

is the Lennard-Jones term which is evaluated only between oxygen sites. An additional interaction term due to induced dipole moments appears in the case of polarizable models, such as PPC (15, 16). In the SPC/E model each water molecule contains three charged sites, a charge of -0.8476 e on the oxygen position and two charges of +0.4278 e on the hydrogen positions placed tetrahedrally at distances of 1.0 Å from the oxygen site. The Lennard-Jones parameters of the SPC/E potential are $\varepsilon_{LJ}$=0.6517 kJ/mol and $\sigma$=3.166 Å.

In straightforward equilibrium NVE (constant density and energy) MD simulation the positions of particles are obtained by solving the Newton's equation of motion

$$F_i(t) = m\ddot{r}_i(t) = -\frac{\partial U(r^N)}{\partial r_i} . \qquad (5)$$

Here, $F_i$ is the force on particle i caused by the N-1 other particles, $r_i$ is its position, the dots indicate the time-derivatives, and m is the mass for particle i. The boundary conditions for the simulated system are largely dictated by the physical situation; for instance, if a bulk liquid or a solid is to be studied, periodic boundary conditions are usually employed (17).

Integrating the equations of motion produces individual trajectories for particles from which the time averages, <A>, for various macroscopic physical-chemical properties can be obtained:

$$\langle A \rangle = \lim_{t \to \infty} \frac{1}{t} \int_0^t A(\tau) d\tau . \qquad (6)$$

In addition to static properties, such as the configurational energy and dielectric constant, pressure, etc., various dynamical properties, such as the relaxation times and transport coefficients (the self-diffusion coefficient and viscosity, etc.), can be calculated. Recent advances in molecular dynamics simulation techniques, known as nonequilibrium molecular dynamics (NEMD), have now made it possible to study computationally dynamical processes as they essentially occur in physical experiments, i.e. the response of a system to applied external fields (18, 19).

Briefly, this NEMD simulation technique utilizes more general non-Newtonian equations of motion which include a perturbation field as part of the statistical-mechanical description. When the applied field does work on the system these equations of motion employ an appropriate thermostatting mechanism to remove the dissipative heat. NEMD has proven to be a particular efficient approach in the studies of collective dynamical phenomena than traditional equilibrium MD methods

(which involve the accumulations of the appropriate time-correlation functions).

## 3. CRYSTALLIZATION OF NONPOLAR MOLECULAR LIQUIDS

Although simulations of the crystallization of simple monoatomic liquids can be performed almost routinely (by simply reducing the temperature), the crystallization of molecular liquids still poses principal difficulties, similar to those encountered in studying protein folding - a large number of translational and rotational degrees of freedom which tend to relax into metastable "traps" of the potential energy surfaces (PES) (20, 21). Metastable disordered ("glassy") states which emerge upon a reduction of temperature usually prevent the nucleation of a regular molecular crystal on a time-scale of a typical simulation. A unique molecular system in which the spontaneous nucleation can be detected upon simple quenching is carbon dioxide, $CO_2$ (7).

We have recently carried out a series of extensive MD simulations of carbon dioxide ($CO_2$) and have observed the spontaneous formation of an fcc (face-centered cubic) crystal from a supercooled liquid on time-scales of $10^{-10}$ to $10^{-9}$ seconds over a narrow range of temperatures. It is worthwhile mentioning that the short-range interactions in the condensed phases of this model carbon dioxide account for approximately 75 % of the total configurational energy, which may explain its susceptibility to crystal formation upon simple quenching.

These MD simulations were performed with samples of 108, 256 and 500 molecules at a constant density of 1.4 g/cm$^3$ and employed the three-site Murthy-Singer-McDonald potential (22), as modified by Geiger *et. al.* (23). Ewald sums (and spherical cut-off for the larger systems) were utilized in cubic periodic boundary conditions to calculate the electrostatic interactions (11). Gaussian isokinetic equations of motion (18) were integrated using a fourth-order Gear algorithm (24) with a time-step of 2.0 fsec.

Samples of supercooled liquid carbon dioxide were prepared at 180 K by rapid cooling a well-equilibrated liquid configuration at 300 K, a temperature well above the estimated mechanical melting point of 240 K, followed by a further equilibration for 200 ps. The resulting configurations of supercooled liquid $CO_2$ at 180 K served as the starting points in a series of MD simulations in which the temperature was further reduced at a rate of 30 deg/psec from 180 K to the desired final value where it was fixed. These deeply quenched liquid samples were then allowed to evolve. The crystallization of carbon dioxide with the density of 1.4 g/cm$^3$ was observed on time-scales of hundreds of picoseconds to a few nanoseconds at temperatures between 70 and 90 K.

Fig. 1 displays the average total configurational energy and the pressure, as a function of time, for the 108 particle carbon dioxide sample quenched to a temperature of 85 K. In Fig. 1 t=0 corresponds to the moment when this temperature was established. Both the energy and the pressure clearly indicate the nucleation event at approximately 750 psec. (0.75 nsec). The "nucleation time" refers to the point along the system's trajectory beyond which the energy and the pressure sharply decrease (see Fig. 1). Similar time-dependencies in the energy and the pressure can be obtained for those samples that eventually undergo crystallization.

A critical question that can be addressed in

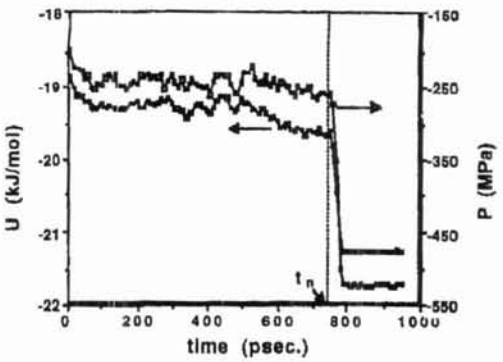


**Figure 1** The time-dependence of the total configurational energy and the pressure for the carbon dioxide sample quenched to a temperature of 85 K. Each point represents a block average taken over 19.0 psec. The nucleation time, $t_n$, is approximately 750 psec.

these simulations is what microscopic changes accompany the liquid to solid phase transition. Fig. 2 displays the carbon-carbon radial distribution functions (RDF), g(r), and the projections, $h^{220}(r)$, of the full pair-correlation function (25) which are useful for examining the average translational and orientational orders in the system, respectively.

The average local structure in the system does not appear to exhibit significant changes until virtually the moment when the nucleation begins at approximately 750 psec. The RDF, g(r), and the projection $h^{220}(r)$ recorded at 10, 200, 400 and 600 psec. after quenching are essentially identical; only a small change in these functions is detectable at t = 700 psec. (see Fig. 2). Representative molecular configurations for this carbon dioxide sample generated at t = 700 psec. and at the completion of the simulation run are shown, respectively, in Figs. 3a and 3b. Fig. 3a illustrates the formation of disordered molecular layers as early precursors of the crystalline heterophase. Detailed analysis of molecular configurations generated in the proximity of the phase transition suggests that both the translational order and the rotational order of the $CO_2$ crystal emerge simultaneously.

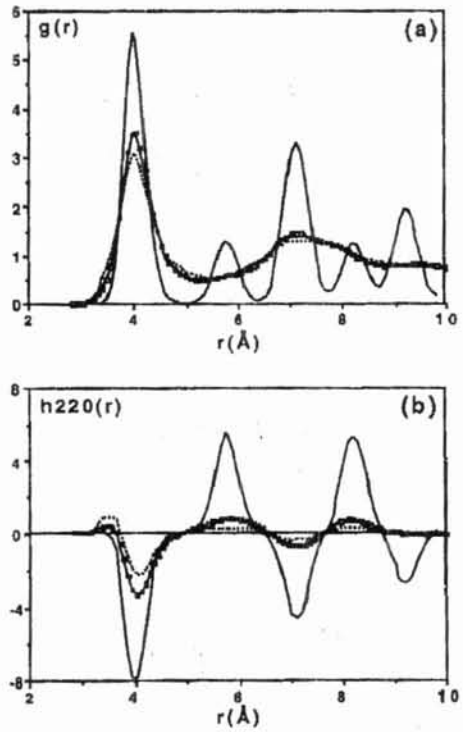


**Figure 2** The local structure in the carbon dioxide sample quenched to a temperature of 85 K at different stages of its liquid to crystalline-solid transition. (a) The carbon-carbon radial distribution functions, g(r); (b) the orientational distribution functions, $h^{220}(r)$. The dotted and the heavy-solid lines portray, respectively, the local structure in the supercooled liquid at the beginning of the simulation run (at t = 10 psec.) and in the resulting crystalline solid. The solid line marked with open squares represents the local structure just prior to crystallization at t = 700 psec.

The critical nucleus (shown in Fig. 4) which arrives in metastable liquid $CO_2$ prior to catastrophic crystal growth features a ramified structure. Apparently, deep quenches in this molecular system initiate the nucleation process that can not be simply described by the classical nucleation theory (9, 10)

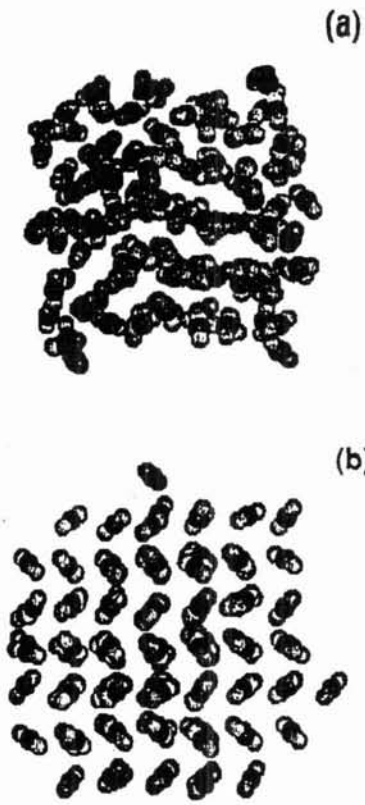


**Figure 3**, Molecular configurations of carbon dioxide at 85 K (a) at t = 700 psec after quenching and (b) at the completion of the simulation run. The black spheres are the carbon atoms and the gray spheres are the oxygen atoms of $CO_2$ molecules.

**Figure 4** Critical nucleus prior to a catastrophic crystal growth.

which portrays critical nucleus as a compact object with well-defined surface.

While the RDF and the projection $h^{220}(r)$ appear rather insensitive to the microscopic changes taking place in the system up to the moment of the phase transition, it is the self-diffusion coefficients that exhibit a more pronounced response. We have examined for the mean self-diffusion coefficient D and its two principal components, $D_\perp$ and $D_\parallel$, characterizing the translational motions of linear $CO_2$ molecules in directions perpendicular and parallel to their principal axes (26). Their values were accumulated (as averages taken over 30 psec.) at various points along the system's trajectory at 85 K and are displayed in Table 1. In the transforming liquid the translational motions of $CO_2$ molecules perpendicular to their axes "freeze" more rapidly than the motions parallel to their axes (compare $D_\perp$ and $D_\parallel$ in Table 1). As a result, the anisotropy in the self-diffusion coefficient as measured by the relative difference of the orthogonal components, $(D_\perp-D_\parallel)/D$, increases three-fold between 400 and 700 psec. We note that the mean self-diffusion coefficient,

**Table 1**

The mean self-diffusion coefficient, D, and its two principal components, $D_\perp$ and $D_\parallel$, obtained during the evolution of a $CO_2$ system at 85 K. Nucleation occurs at approximately 750 psec.

| time psec | $Dx10^6$ $cm^2/sec$ | $D_\parallel x10^6$ $cm^2/sec$ | $D_\perp x10^6$ $cm^2/sec$ | $(D_\perp-D_\parallel)/D$ |
|---|---|---|---|---|
| 10 | 1.7 | 1.9 | 1.6 | 0.18 |
| 200 | 1.5 | 1.7 | 1.4 | 0.2 |
| 400 | 1.5 | 1.7 | 1.4 | 0.2 |
| 600 | 0.52 | 0.64 | 0.42 | 0.4 |
| 700 | 0.33 | 0.47 | 0.26 | 0.6 |

$D=1/3(2D_{\perp}+D_{\parallel})$, decreases almost 5-fold during the same time-period. Clearly, the development of directional anisotropy in the local molecular diffusion is crucial in the nucleation process.

Nucleation times when plotted versus final temperature indicate the existence of a minimum in the time for crystal formation at a specific temperature (in the case of $CO_2$ near 75 K), as can be seen in Fig. 5a. It is interesting to note that this feature of the crystal nucleation dynamics has been predicted by the classical nucleation theory.

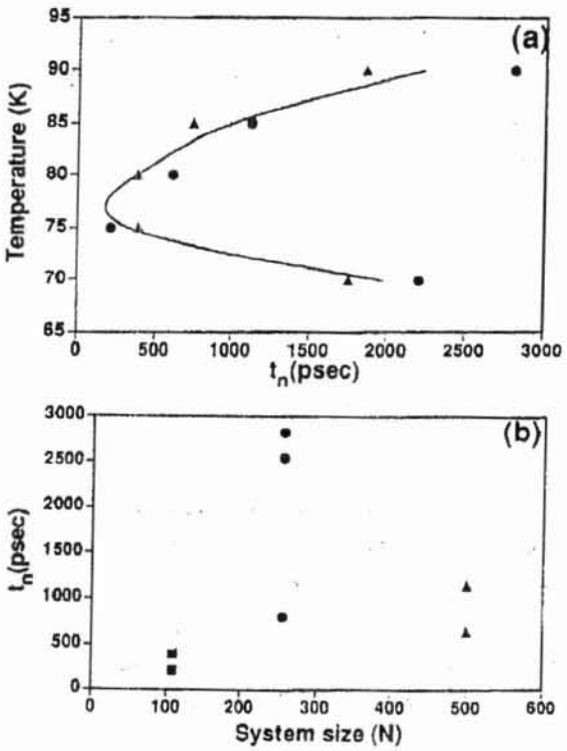


**Figure 5** (a) The nucleation times, $t_n$, for 108 particle samples of carbon dioxide at a density of 1.4 g/cm$^3$. In this TTT (time-temperature-transformation) plot the triangles and circles are results obtained in two independent series of simulations (b) The system size effects in the nucleation times. The squares, circles and triangles are values observed for 108, 256 and 500 particle samples, respectively, of carbon dioxide at a density of 1.4 g/cm$^3$ quenched to a temperature of 75 K.

Several simulations have been carried out with systems of 256 and 500 molecules to examine the influence of the sample size. These results are shown in Fig. 5b. Following the same preparatory procedure, rapid quenching of three independently equilibrated 256 particle samples from 180 to 75 K resulted in their crystallization at 0.8, 2.54 and 2.8 nsec., respectively, representing approximately a 5-fold increase in the mean nucleation time when compared with 108 particle samples. It is worthwhile noting that similar sample size effects have been previously observed by Honeycutt and Andersen in their MD simulation study of simple atomic Lennard-Jones systems (27). Spontaneous crystallization in 500 particle samples was observed at times that are smaller than those obtained for N=256. This observation indicates that with a 500 particle $CO_2$ sample the process of the catastrophic crystal growth from the metastable liquid is becoming less biased by the periodic boundary conditions.

The crystals of carbon dioxide obtained in these simulations feature the same regular fcc packing of carbon atoms found experimentally (28), as can be seen in Fig. 3b. They occasionally exhibit some rotational defects (but obviously not the rotational disorder found in plastic crystals), in accord with experimental observations which indicate the presence of some rotational defects in real $CO_2$ crystals (29). A rotational phase transition into a plastic crystal (30) before (translational) melting has been found, for instance, in solid $N_2$, making it an interesting candidate for computer simulations.

Aside carbon dioxide, only a few other nonpolar molecular systems have been successfully crystallized in a molecular dynamics simulation. Recently, Gray and co-workers (31) have reported

upon the possibility of crystallization of simple molecular fluids through shear-induced nucleation. In their work with diatomic and triatomic Lennard-Jones fluids they have imposed a linear velocity gradient normal to the flow direction, thus simulating planar shearing flow. It has been found that positional ordering takes place even when orientational ordering is not in evidence, and the subsequent transition on cooling from a positionally ordered system to a fully crystalline state takes place with ease. Their theoretical estimates suggest that thermally induced shear fluctuations of sufficient magnitude to induce ordering may occur in equilibrium systems.

Also, Esselink and co-workers (32) have performed extensive MD simulations of melting and freezing of the chain Lennard-Jones molecules representing n-alkanes (ranging from butane to dodecane). Starting from amorphous phases they have observed an ordering, consistent with hexagonal packing. Their results seem to indicate that smaller chains crystallize slower, with butane as an extreme example.

## 4. ENHANCED SAMPLING IN MD SIMULATIONS OF CRYSTALLIZATION

Significant savings of computer time in the studies of crystallization can be achieved by using various sampling techniques which help enhance (accelerate) the configurational search through a coarse graining of the phase space, by lowering the potential barriers between local minima on the PES. Simulated annealing is the most straightforward approach that can be used to improve sampling of the PES. In recent years a variety of refined techniques, such as umbrella sampling, multicanonical sampling, genetic algorithms, force (anti-force)-biased methods, etc., has been implemented, both in Monte Carlo (MC) and molecular dynamics (MD) simulations (33-37).

In this paper we describe a simple and practical method with which to perform an enhanced configurational sampling in molecular dynamics simulations, our main goal being to achieve a faster crystallization of a supercooled $CO_2$.

A faster crystallization of a supercooled molecular liquid can be accomplished by inducing small stochastic perturbations to the intermolecular potential as the system moves along its phase space trajectory. In this method, the intermolecular potential for the system, u(r), is scaled at each MD time-step by a random number, $\alpha$,

$$u_n(r)^* = \alpha_n\, u(r), \qquad (7)$$

so that

$$\langle u_n(r)^* \rangle = \langle \alpha_n \rangle u(r) = u(r), \qquad (8)$$

where $u_n(r)^*$ and $\alpha_n$ are, respectively, the scaled intermolecular potential and its scaling multiplier at the time-step n, <...> denotes the usual ensemble average, and the first equality in Eq. (8) follows from the requirement that $\langle \alpha_n \rangle = 1$. The numerical value for $\alpha$ is determined through a recurrent random walk procedure around unity where each step of the random walker is performed at each new MD step. Essentially, this approach combines a stochastic sampling in the parameter space for the interaction potential with the regular MD procedure.

Formally, the restricted random walker $\alpha$, or the potential multiplier, can be defined as

$$\alpha_{n+1} = \alpha_n + \Delta\alpha_{n+1} \qquad (9)$$

and

$$\Delta\alpha_{n+1} = \sigma\,(2\,R - \alpha_n)\,, \qquad (10)$$

where $\alpha_{n+1}$ is the potential multiplier at the next, (n+1), time-step, $\Delta\alpha_{n+1}$ is the size of the step of the random walker, R is the random number generated in the interval [0, 1] and $\sigma$ is the numerical constant determining the width of the distribution sampled by $\alpha$. We remark that thermostated equations of motion can accommodate these small stochastic perturbations to the regular intermolecular forces since at each time-step the random force experiences only a small change in magnitude.

The nucleation times appear to depend significantly on $\sigma$. In particular, using $\sigma = 0.0015$ (to determine the width of the sampling distribution for $\alpha$) results in approximately a three-fold reduction in the crystallization time, as compared with the standard ($\sigma = 0$, $\alpha \equiv 1.0$) simulations. The induced stochastic forces are typically less than 1% of those resulting from the intermolecular interactions (i.e. $\alpha$ fell within the range 0.99 and 1.01).

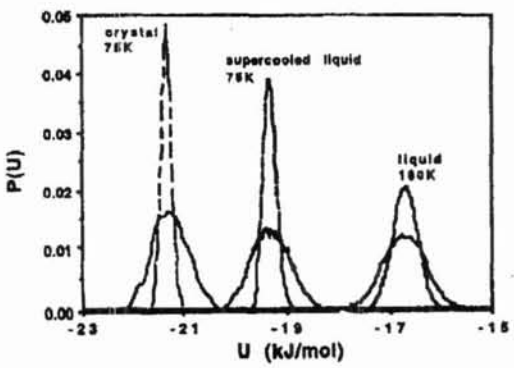


**Figure 6** The potential energy distributions for carbon dioxide system accumulated in a standard MD simulation (the broken lines) and in a simulation with $\sigma = 0.0015$ (the solid lines). Liquid carbon dioxide at 180 K, supercooled liquid at 75 K prior to the nucleation event and crystal that emerges from this liquid after the nucleation are represented.

A notable feature of this simulation method is that it preserves the canonical (Gaussian) form for the potential energy distribution, P(U). Fig. 6 displays the potential energy distributions for liquid $CO_2$ at 180 K accumulated in a standard MD simulation and in a simulation with $\sigma = 0.0015$; at this temperature the system is far from phase instabilities. Also shown in Fig. 6 are the results obtained at 75 K for supercooled liquid prior to the nucleation event and for crystal that emerges from this liquid after the nucleation.

The incorporation of a random energy scaling, or a perturbing random force effectively increases the energy fluctuations experienced by the system, yet without changing average properties such as the energy or pressure. The resulting potential energy distribution for an equilibrium system $P(\alpha U)$, broadened by a restricted random walk in $\alpha$, can be deconvoluted back to the original distribution , P(U), since

$$P(\alpha U) = \int_{-\infty}^{\infty} P(U)P(\alpha)d\alpha. \qquad (11)$$

This broader energy distribution must span more configurational states of the system. Random, yet small, distortions (perturbations) of the PES enable the trajectory to escape metastable "traps" by making accessible those high (and hence low) energy configurations that would not be normally sampled through the inherent thermal fluctuations, eventually leading to a faster nucleation.

## 5. ELECTROFREEZING OF WATER

The crystallization of liquid water plays a fundamental role in many natural and technological processes (38). It is now well-documented that a

geometric match between the microscopic structure of a substrate surface and the ice structure can help to facilitate ice nucleation at the surfaces of various materials. However, reports have persisted of another important mechanism with which nature controls the freezing of water. As various observations have indicated, some dating from the previous century, an electric field can promote the nucleation of ice from supercooled liquid water. This electrofreezing effect plays an important role in many natural processes, ranging from tropospheric dynamics to frost damage to cells (39, 40). It has been argued that local electric fields have the ability to induce the crystallization of liquid water at surfaces which can be distinctly different from those of ice (41).

Using computer simulations we have examined electric field effects on the phase behavior of low-temperature water, and have discovered that an applied homogeneous static electric field can indeed induce crystallization of the supercooled liquid. In computer simulations of water, a highly polar substance, the application of an electric field facilitates the nucleation of polar ice from the metastable liquid (as it appears to in nature) providing a unique opportunity to study directly the process of crystallization of water at the molecular level.

This paper reviews the electrofreezing of water as modeled with the TIP4P and SPC/E potentials; both have been shown to describe reasonably successfully the properties of the real liquid and various amorphous and crystalline ices (42, 43). Most of the work has been carried out with 256 and 64 particle samples, respectively, in truncated octahedral and cubic simulation cells. It is clear from symmetry considerations that both truncated octahedral and cubic samples with N = $1/2(4n^3)$ and $8(n^3)$, respectively, where n=1, 2, 3, ... will accommodate an ice $I_c$ lattice in periodic boundary conditions. The Ewald summation technique was used to evaluate the long-range electrostatic interactions. A fourth-order Gear algorithm with a time step of 1.25 fsec was used to integrate the equations of motion in which the rotational degrees of freedom were represented using

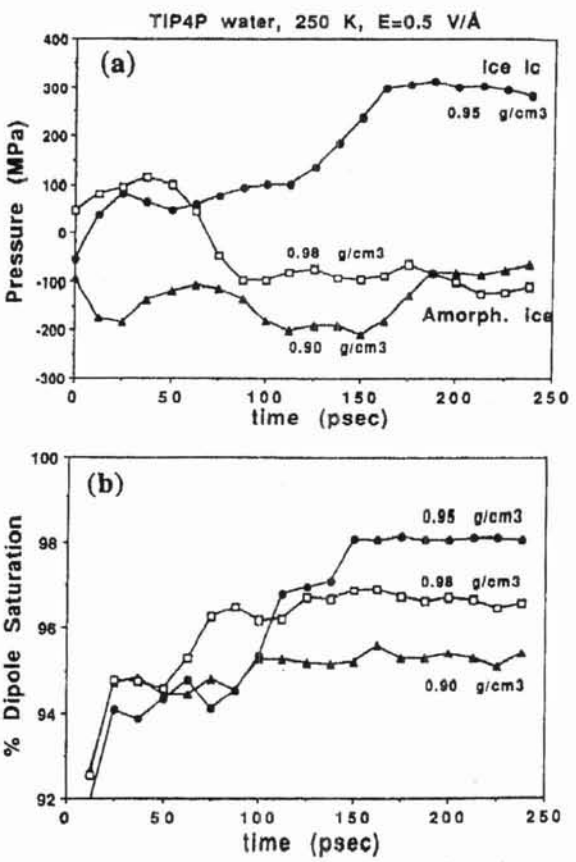


**Figure 7** The time-dependence for (a) the pressure and (b) the % dipole saturation in TIP4P water samples with different densities subjected to an electric field. Each point represents a block average taken over 12.5 psec. All data are at a temperature of 250K for a field of 0.5 V/Å. The values at t=0 represent field-off conditions.

quaternions. Applied electric fields were typically between 0.1 and 0.5 V/Å. These fields are smaller than the average local (internal) electric fields within condense phases of water (which range around 1.5-2.0 V/Å). These values also lie within the operating range of modern lasers (44) and are comparable with the local electric fields experienced by water molecules near the surfaces of biopolymers.

Figs. 7a-b display, respectively the pressure and the % dipole saturation of several water samples as a function of time. The % dipole saturation is defined as $(100\% \cdot M) / (N \cdot \mu)$, where M is a total dipole moment of a sample, N is the number of particles and $\mu$ is the dipole moment of the water molecules. In this Figure t=0 corresponds to the moment when the field was applied. Typical results obtained at temperature of 250 K and densities of $\rho$ = 0.90, 0.95 and 0.98 g/cm$^3$, respectively, are shown.

The field-induced crystallization of liquid TIP4P water into ice I (7, 45) takes place within a small range of densities around 0.95 g/cm$^3$ at T = 250 K, on a time-scale of a few hundred picoseconds. Upon application of the electric field these supercooled liquids appear to transform rapidly, within 50-80 psec., into amorphous-like (layered) materials. After approximately 120 psec. the pressure in these water samples increases markedly indicating a change of phase. At the same time their microscopic structures begin to demonstrate the features of a regular crystalline solid. At 160-200 psec. after the application of the field the pressure curves plateau marking the point beyond a new crystalline phase exists. The polar ice crystal that emerges at this stage still possesses numerous lattice defects and will melt if the electric field is removed. Melting of this imperfect ice crystal in the absence of applied field can be avoided by quenching it to a temperature of 200 K. In the continued presence of the field, lattice defects tend to disappear, usually after a further 100-200 psec., and the resulting crystal is stable at T = 250 K in the absence of the field. As one might expect the resulting crystalline samples attain a substantially lower energy and a higher degree of the dipole saturation than any amorphous samples at the same temperature. Fig. 8 visualizes specific molecular configurations generated during the process of ice nucleation.

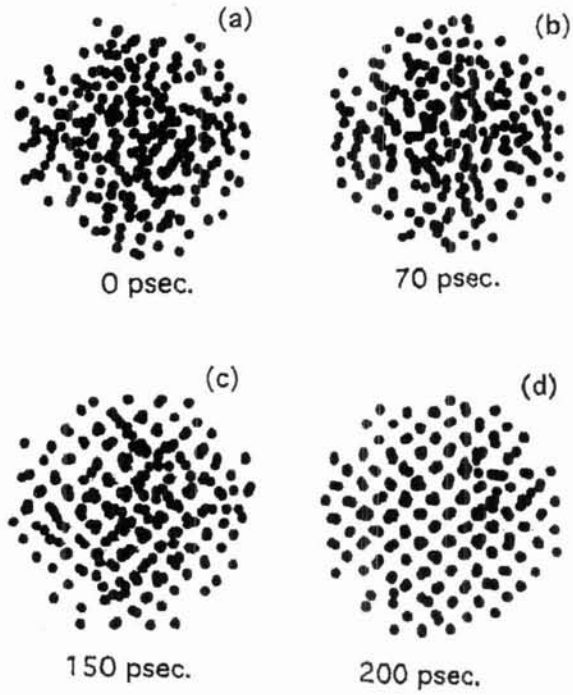


**Figure 8** Molecular configurations of a water system generated during a field-induced phase transition. (a) Initial liquid water configuration. (b), (c) and (d) Applied-field results at different stages of ice formation. The dots represent the oxygen atoms of the water molecules. The applied field is acting along the normal to the plane of the Figure. All data are at 250 K for a field of 0.5 V/Å.

Fig. 8d displays the structure of a polar crystal formed from supercooled liquid TIP4P water at temperature of 250 K and density of 0.95 g/cm$^3$ This structure can be identified as cubic ice I. Although hexagonal ice is the predominant crystalline form of water encountered on the Earth, the crystallization of liquid water into cubic ice can be also observed; it has been argued that formation of cubic ice is kinetically favored under certain conditions. Small droplets of water in the upper atmosphere often freeze into cubic ice (46). In the laboratory cubic ice has been obtained by freezing liquid water in porous materials, by vapor-deposition, by warming amorphous and high-pressure crystalline ices and by freezing very large clusters of water in supersonic flow (47-49). As noted recently by Xia and Berkowitz (50), water layers next to the surface of charged Pt walls tend to acquire a cubic ice structure.

Simulation results reveal a remarkable similarity between the low-density amorphous ice and the disordered structures appearing at intermediate stages during crystallization of water. This sample consists of stacked molecular layers with numerous planar defects and long-range disorder within the layers. The local structure in this disordered material is characterized by a tetrahedral four-coordinated arrangement of hydrogen-bonded molecules. It does not exhibit the "interstitially" coordinated molecules peculiar to the local structure in liquid water at ambient conditions (51, 52) and high-density amorphous ice (53). An analogous packing pattern characterizes the low-density amorphous ice (53). We recall (51-52) that the interstitial coordination of $H_2O$ molecules accounts for the elevated pair-density in the region of the first minimum in the radial distribution function (RDF) of oxygen atoms, $g_{OO}(r)$, for liquid water and high-density amorphous ice at about 3.5 Å. In the spatial distribution function, $g_{OO}(r, \Omega)$, which represents the spatial analog of the RDF, this "interstitial" coordination appears as local maxima at nontetrahedral positions at separations of about 3.3-

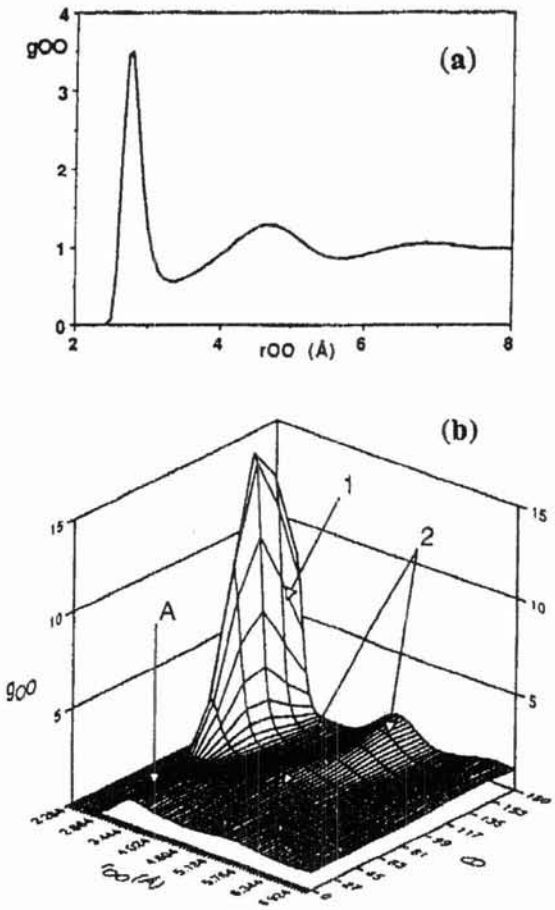


**Figure 9** The local structure in the supercooled liquid water at 250 K. (a) The radial distribution functions of oxygen atoms (b) The spatial distribution function of oxygen atoms. θ denotes the angle between the dipole axis of the central water molecule and the oxygen-oxygen separation vector. 1 and 2 identify, respectively, the first and the second tetrahedrally bonded neighbors of the continuous H-bond network, and A represents nontetrahedral (interstitial) coordination.

3.9 Å. The representative local spatial distributions of oxygen atoms in liquid water and cubic ice are shown in Figs. 9 and 10; the detailed analysis of local order in condensed phases of water can be found elsewhere (6, 51-53).

These Figures provide direct evidence that the interstitial nontetrahedral coordination in liquid water, a local maximum in the spatial distribution function, $g_{OO}(r, \Omega)$, at approximately 3.3-3.9 Å (see Fig. 9b), disappears when the supercooled liquid transforms into an ice (see Fig. 10b). These interstitially coordinated molecules in water structure must clearly play a crucial role in characterizing the liquid water to ice transition.

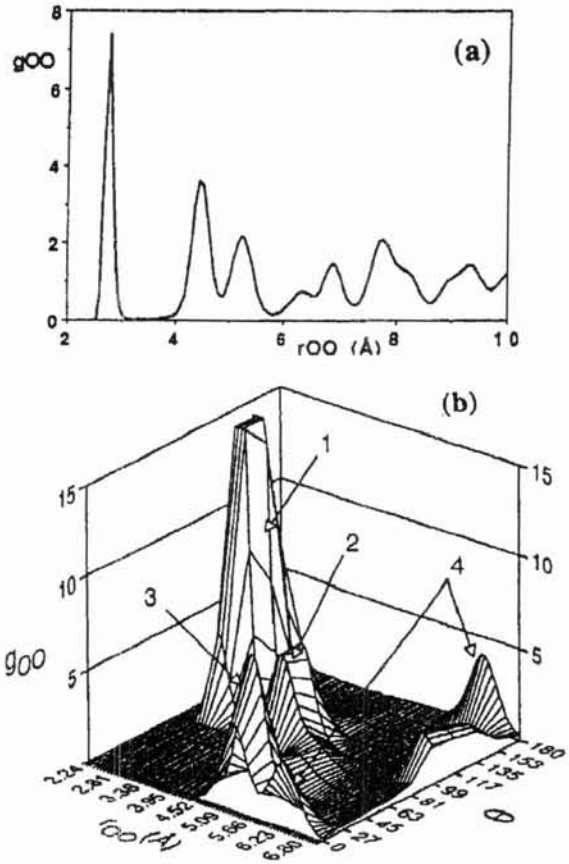


**Figure 10** The local structure in the ice I at 100 K. (a) The radial distribution functions of oxygen atoms (b) The spatial distribution function of oxygen atoms θ denotes the angle between the dipole axis of the central water molecule and the oxygen-oxygen separation vector. 1, 2, 3 and 4 identify, respectively, the first, the second, the third and the fourth tetrahedrally bonded neighbors of the continuous H-bond network.

Another distinctive structural change evident from the spatial distributions of oxygen atoms is associated with the second (H-bonded) neighbors (identified as 2 in Figs. 9 and 10). In the supercooled liquid these neighbors appear over a wide range of orientations in the local frame. During the phase transition they collapse onto distinctive sites in the local frame giving rise to a sharp pair-density maximum in the SDF (see Fig. 10b). Moreover, the third and fourth (H-bonded) neighbors which are virtually undetectable in the liquid water SDF (Fig. 9b) appear as well defined maxima in Fig. 10b (labeled as 3 and 4). We remark that for a crystalline solid the SDF representing O...O correlations exhibits tetrahedral symmetry; for example, the function $g_{OO}(r, \Omega)$ in the plane of the central molecule (i.e., $\phi$=0) is equivalent to the out-of-plane result shown in Fig. 10b. This is not true in the liquid state.

The influence of temperature upon the crystallization of TIP4P water was examined using samples with densities of 0.95 g/cm$^3$ and an applied field of 0.5 V/Å. At temperatures above 250 K the regular solid produced by the field always exhibited some disorder, the thermal motion of the water molecules allowing for rapid formation and removal of local lattice defects. Ice crystals obtained from more deeply supercooled water samples (at or below T=230 K) were found to contain defects which the applied field was unable to eliminate over the

observation time. One possible explanation for their persistence is that at low temperatures the higher viscosity of original liquid prevents the proper orientation of (and in) the nucleation seeds.

Recently, Borzsak and Cummings (54) have investigated the effect of an oscillatory shear in a combination with electric field on the freezing of water. They find that the simple step of adding oscillatory shear is a very useful tool in the simulations of freezing, resulting in a order of magnitude faster crystallization.

The application of an electric field to liquid TIP4P water under pressures of 3-5 kbar and at temperatures of 225-240 K produces a new ice polymorph with an open quartz-like structure (hereafter ice XII), on a time-scale of typically 1 nsec (55). Water expands upon freezing into this structure, as it does during the nucleation of ice I which also features an open crystalline packing. The crystal structure of ice XII in its minimum energy configuration at 150 K has the density of 1.14 g/cm$^3$ and is shown in Fig. 11.

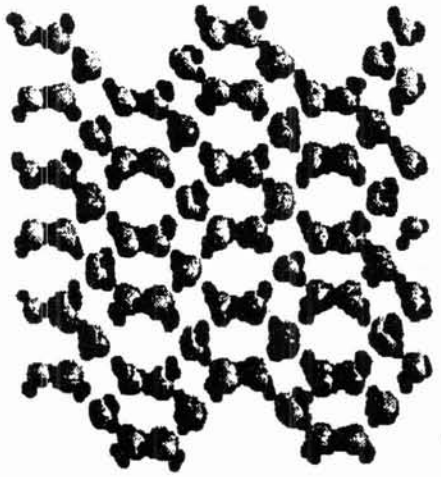

**Figure 11** The structure of ice XII at 150 K and 2 kbars. The gray and the black spheres represent, respectively, the oxygen and the hydrogen atoms of the water molecules.

Each water molecule in the structure of ice XII has four nearest hydrogen (H) bonded neighbors at distances of 2.71-2.75 Å. An important structural feature of ice XII distinguishing it from the known higher density crystalline forms of water is the absence of interstitially coordinated molecules. Independently, Baez and Clancy (56) have suggested that a similar quartz-like ice structure may be the thermodynamically preferred solid structure for SPC/E water at low and moderate pressures.

## 6. CONCLUDING REMARKS

Crystallization of molecular liquids has many practical consequences in science and technology. In recent years, new computational techniques have been developed to study the microscopic dynamics of this process. Molecular dynamics simulations provide crucial insights into various microscopic transformations occurring at different stages of crystal nucleation. Despite these recent advances much remains to be accomplished. What is clearly needed is analysis of theoretical and experimental nucleation rates and critical nuclei in a variety of systems, in terms of molecular parameters. Aside their fundamental theoretical interest, these studies promise new advances in areas such as materials design and modification.

## ACKNOWLEDGMENTS

We are grateful for the financial support of the Natural Sciences and Engineering Research Council of Canada.

## REFERENCES

1. Frenkel D. and McTague J.P. 1980

Ann.Rev.Phys.Chim. 31, 491.
2. Swope W.C. and Andersen H.C. 1990 Phys.Rev. B 41, 7042.
3. Laird B.B. and Haymet A.D.J. 1992 Chem.Rev. 92, 1819.
4. Klein W. 1991 In: Springer Proceedings in Physics, 53, 50.
5. Rahman A., Mandel M.J. and McTague J.P. 1976 J.Chem.Phys. 64, 1564.
6. Svishchev I.M. and Kusalik P.G. 1994 Phys.Rev.Lett. 73, 975.
7. Svishchev I.M. and Kusalik P.G. 1995 Phys.Rev.Lett. 75, 3289.
8. Bartell L.S. 1995 J.Phys.Chem. 99, 1080.
9. Oxtoby D.W. Adv.Chem.Phys. 1988 70, 263.
10. Oxtoby D.W. 1992 J.Phys.:Condens.Matt. 4, 7627.
11. Allen M.P. and Tildesley D.J. 1987 Computer Simulations of Liquids, Oxford University, Oxford.
12. Rapaport D.C. 1995 The Art of Molecular Dynamics Simulation, Cambridge University, Cambridge.
13. Jorgensen W.L., Chandrasekhar J., Madura J.D., Impey R.W. and Klein M.L. 1983 J.Chem.Phys. 79, 926.
14. Berendsen H.J.C., Grigera J.R. and Straatsma T.P. 1987 J.Phys.Chem. 91, 6269.
15. Svishchev I.M., Kusalik P.G., Wang J. and Boyd R.J. 1996 J.Chem.Phys. 105, 4742.
16. Rick S.W., Stuart S.J. and Berne B.J. 1994 J.Chem.Phys. 101, 614.
17. Fincham D. and Heyes D.M. 1985 Adv. Chem. Phys. 63 , 493.
18. Evans D.J. and G.P. Morriss G.P. 1990 Statistical Mechanics of Nonequilibrium Liquids, Academic, San Diego.
19. Svishchev I.M. and Kusalik P.G. 1993 Physica. A 192, 628.
20. Stillinger F.H. 1990 Phys.Rev. B 41, 2409.
21. Doye J.P.K. and Wales D.J. 1998 Phys.Rev.Lett. 80, 135.
22. Murthy C.S., O'Shea S.F. and McDonald I.R. 1983 Mol. Phys. 50, 531.
23. Geiger L.C., Ladanyi B.M. and Chapin M.E. 1990 J.Chem.Phys. 93, 4533.
24. Evans D.J. and Morriss J.P. 1984 Comp. Phys. Rep. 1, 297.
25. Stell G, Patey G.N. and Hoye J.S. 1981 Adv.Chem.Phys. 48, 183.
26. Svishchev I.M. and Kusalik P.G. 1994 J.Phys.Chem. 98, 728.
27. Honeycutt J.D. and Andersen H.C. 1984 Chem.Phys.Lett. 108, 535.
28. Kitaigorodsky A.I. 1973 Molecular Crystals and Molecules, Academic, New York.
29. Manzheli V.G., Tolkachev A.M., Bagatskii M.I. and Voitovich E.I. 1971 Phys. Status Solidi B 44, 39.
30. Scott T.A. 1976 Phys. Rep. 27C, 89.
31. Gray et.al. 1995 Proc.R.Soc.Lond.A 448, 113.
32. Esselink et.al. 1994 J.Chem.Phys. 101, 9040.
33. Kirkpatrick S., Gelatt C.D. and Vecchi M.P. 1983 Science 220, 671.
34. Wolynes P.G., Omuchic J.N. and Thirumalai D. 1995 Science 267, 1619.
35. Hansmann U.H., Okamoto Y. and Eisenmenger F. 1996 Chem.Phys.Lett. 259, 321.
36. Bartels C. and Karplus M. 1998 J.Phys.Chem. 102, 865.
37. Borgis D. and Staib A. 1996 J.Chem.Phys. 104, 4776.
38. Eisenberg D. and Kauzmann W. 1969 The Structure and Properties of Water, Oxford University Press, Oxford.
39. Tinsley B.A. 1994 EOS, Trans. AGU, 75, 369.
40. Kajava A.V. and Lindow S.E. 1993 J.Mol.Biol. 232, 709.
41. Gavish M., Popovitz-Biro R., Lahav M. and Leisterowitz M. 1990 Science 250, 973.
42. Tse J.S. and Klein M.L. 1987 Phys.Rev.Lett. 58, 1672.
43. Poole P.H., Sciortino F., Essmann U. and Stanley H.E. 1992 Nature 360, 324.
44. Zhu S.-B., Singh S. and Robinson G.W. 1994 Adv.Chem.Phys. 85, 627.
45. Svishchev I.M. and Kusalik P.G. 1996 J.Am.Chem.Soc. 118, 649.
46. Mayer E. and Hallbrucker A. 1987 Nature 325, 601.
47. Steytler D.C., Dore J.C. and Wright C.J. 1983 J.Phys.Chem. 87, 2458.
48. Bartell L.S. and Huang J. 1994 J.Phys.Chem. 98, 7455.
49. Hage W. Hallbrucker A. Mayer E. and Johari J.P. 1994 J.Chem.Phys. 100, 2743.
50. Xinfy Xia and Berkowitz M.L. 1995 Phys.Rev.Lett. 74, 3193.
51. Svishchev I.M. and Kusalik P.G. 1993 J.Chem.Phys. 99, 3049.
52. Svishchev I.M. and Kusalik P.G. 1994 Science 265, 1219.
53. Svishchev I.M. and Kusalik P.G. 1995 Chem.Phys.Lett. 239, 349.
54. Borzsak I and Cummings P.G. 1997 Phys.Rev. B 56, R6279.
55. Svishchev I.M. and Kusalik P.G. 1996 Phys.Rev. B 53, R8815.
56. Baez L.A. and Clancy P. 1995 J.Chem.Phys. 103, 9744.